J Mater Sci (2007) 42:8222–8229
DOI 10.1007/s10853-007-1695-6

Preparation of smooth potassium hexatitanate nanofilms by sol–gel method

Q. H. Qian · X. F. Zhou · Y. Y. Hu · Ch. Liu · X. Feng · X. H. Lu

Received: 16 August 2006 / Accepted: 15 March 2007 / Published online: 19 June 2007

Abstract New nanosmooth potassium hexatitanate films have been prepared on crystalline Si (111) and ITO glass substrates by sol–gel method using $Ti(n\text{-}OC_4H_9)_4$ and CH_3COOK as precursors. Atomic force microscopy (AFM) topographic images were analyzed to select the optimal preparation conditions for the films. It is shown that the films consist of flat particles with the ratio of diameter to height around 11. The root mean square (RMS) roughness of the films based on the measurement of an area of 2,000 nm × 2,000 nm in AFM images is 6.4 nm. The crystal growth process of potassium hexatitanate film was characterized by XRD, Raman spectra, and TEM. The results showed that the crystal growth of potassium hexatitanate nanofilm is a confined growth mechanism. Electrochemical measurements demonstrated that the photocurrent of potassium hexatitanate film electrode is more stable than that of TiO_2 film electrode.

Introduction

Titanates, as the well-known functional materials, have received extensive investigation [1–5] because of their outstanding electronic, magnetic, optical, catalytic, mechanical properties and thermal stability. Among all titanates, alkali metal titanates are of great interest in many important applications such as ion-exchanger [6–8], photoluminescence [9], photochemical catalyst [10, 11], inorganic–organic nanocomposite materials [12], and reinforcing agents for the composite [13, 14]. Potassium hexatitanate with tunnel structures is of particular importance due to its photocatalysis and chemical stability [15]. For example, potassium hexatitanate whisker has been proven to be a suitable substitute for asbestos [16] in alkaline fuel cells because asbestos has been shown to be harmful and carcinogenic and tends to degrade in alkaline solutions. These properties and applications are related to the morphology, size, and crystallinity of potassium titanates. However, the studies of potassium hexatitanate mainly focus on powder and fiber forms of potassium titanates. Few works are reported for potassium titanate films. The difficulty usually lies in the difference of the types of reactions that deposit metal or metal oxides on the substrate from its dissolved precursor.

Films have unique physical and chemical properties which are different from that of bulk materials due to the formation of thin crystalline, noncrystalline, or metastable substances that have size quantization effect and high surface free energy. Films prepared by sol–gel method are usually composed of a polycrystalline mixture. The mesoscopic structure of polycrystalline materials determined their properties, while AFM is an effective instrument for studying the meso-structure of polycrystalline materials since some surface properties of film can be measured through the analysis of AFM images. Therefore, it is necessary to prepare smooth nanofilms in order to study the connection between structure and property. In addition, the mesoscopic structure plays an important role in the application of materials.

Many methods have been developed to prepare films, including sputtering [17], CVD [18], sol–gel [19], atomic layer deposition [20]. Among all the methods, sol–gel route has many advantages, including easy control of the

Q. H. Qian · X. F. Zhou · Y. Y. Hu · Ch. Liu · X. Feng · X. H. Lu (✉)
College of Chemistry and Chemical Engineering,
Nanjing University of Technology, Nanjing 210009, China
e-mail: xhlu@njut.edu.cn

composition, excellent homogeneity on the molecular, even atom level, the ability to coat large area of high quality thin film and low crystallization temperature. Although the films can be prepared by powder coating, the method may result in many defects such as coarse surface and infirm force between the films and substrates. Hence, we hope that potassium titanate films with new functions such as efficient photoelectric energy conversion, photocatalytic activities and better stability in alkaline solution can be prepared through sol–gel routes.

This work focuses on the synthesis and characterization of smooth potassium hexatitanate film. The morphology and surface microstructure were examined by AFM, SEM, and TEM techniques. The surface roughness of potassium hexatitanate films obtained from the analysis of AFM images was used as the criteria to select the optimal preparation conditions of the smooth films. The surface structures in nanoscale were investigated by AFM in detail. Photoelectrochemical properties of potassium hexatitanate film were explored. Similar measurements were carried out on anatase film electrodes with the same thickness for comparison.

Experiments

All analytical grade reagents were used without further purification.

Preparation of TiO_2 films

TiO_2 films were prepared by tetrabutyl titanate (Ti(n-$OC_4H_9)_4$, Shanghai, China) hydrolysis in alcoholic solution and dip-coating method. Ti(n-$OC_4H_9)_4$ was added into anhydrous ethanol under stirring. The pH value of the solution was adjusted by adding HNO_3. A mixture of deionized water and acetylacetone was added into the former Ti(n-$OC_4H_9)_4$ solution drop by drop. The chemical composition of the alkoxide solution was n(Ti(n-$OC_4H_9)_4$):n(C_2H_5-OH):n(H_2O):n($CH_3COCH_2COCH_3$) = 1.0:26.4:2.0:0.5 in molar ratio. Prior to the film deposition, ITO glass (~15Ω/square, Shenzhen, China) was treated by acetone and alcohol and dried thereafter. TiO_2 film was deposited at a rate of 35 mm/min, followed by dehydration at 100 °C. In order to prepare thicker films, the deposition/heat-treatment cycle was repeated six times. Finally, the film was heated to 500 °C at a rate of 3 °C/min and kept for 90 min. After that it was cooled down to room temperature in furnace.

Preparation of potassium hexatitanate films

Acetylacetone and acetic acid were used as chelating agent and solvent, respectively. 2-methoxyethanol (CH_3OCH_2-CH_2OH) was used as diluting agent to get crack free films. First, potassium acetate (CH_3COOK, 92% purity, Shanghai, China) was dissolved in acetic acid. Second, a stoichiometric amount of Ti(n-$OC_4H_9)_4$ was mixed with acetylacetone, followed by the dropwise addition of acetate solution with continuous stirring. After stirring for 2 h, thin yellow homogeneous sol was formed. The molar ratio of various components in sol is n(Ti(n-$OC_4H_9)_4$):n(CH_3COOK):n(CH_3COOH):n($CH_3COCH_2COCH_3$) = 3.0:1.0:5.0:0.5. The sol was heated at 70 °C to form gel for TG-DSC analysis. Third, the gel was grounded and calcined at different temperatures for 2 h in a muffle. Finally, potassium titanate powder was obtained to determine crystal phase and composition.

The clear sol was diluted with 2-methoxyethanol to adjust the viscosity and surface tension. The films were coated onto silicon with ITO glass as substrates by dip-coating. First, the substrates which were cleaned by ultrasonic in a mixture of acetone and alcohol, were lowered into the prepared sol and, withdrawn at a regular rate of 35 mm/min. Second, the wet films were preheated on a hot plate at 350 °C for 10 min. Third, the deposition/heat-treatment cycle was repeated six times. Finally, the coatings were sintered at 600 °C. Calcinations were performed in a muffle furnace with the heating rate of 5 °C/min.

Characterization

Thermal analysis (TG-DSC, Model SDT 2960, TA Instruments, New Castle) was performed on the dried gel with a series of heating rates from 20 °C/min up to 1,000 °C/min in flowing nitrogen gas. X-ray powder diffraction patterns were obtained by using a D8 advance (Bruker AXS, Karlsruhe, Germany). Cu-Kα radiation with a nickel filter and a zero-background sample cell were used, operating at 40 kV and 20 mA. All samples were measured in the continuous scan mode at 5–60°(2θ) with a scanning rate of 0.05°(2θ)/s. Morphologies and surface microstructure of films were characterized by SEM (Model JSM-6300, JEOL, Tokyo, Japan) and AFM (AutoCP-Reaserch, PSI, USA). A JECS-2100 (Japan) transmission electron microscope (TEM) was used to measure the particle size. For TEM investigations, small fragments obtained from scraping thin film samples were sonicated in distilled water for 20 min. The resulting solution was dipped onto a piece of Cu net followed by TEM analysis. Raman spectra were collected using a JY Horiba LabRam HR800 microRaman spectrograph at room temperature.

Electrochemical measurements

All electrochemical experiments were performed using an EG&G PARC Versastat Electrochemical System at room temperature. A 20 ml electrochemical cell is filled with

saturated calomel electrode (SCE) as reference electrode, platinum sheet as auxiliary electrode and potassium hexatitanate film/ITO or titania film /ITO as working electrode. The 0.1 mol/l Na_2SO_4 solution purged with ultrapure N_2 for at least 30 min prior to use was employed as the supporting electrolyte in the electrochemical measurements. The working electrode with a test surface of 1.0 cm^2 was used for all experiments. An 8 W middle pressure mercury lamp with a wavelength centered at 254 nm was used as an illuminant. The intensity of UV light was kept at 2.5 mW/cm^2 in all experiments.

Results and discussion

Thermal analysis

Figure 1 shows the TG-DSC curves for $Ti(n\text{-}OC_4H_9)_4$-CH_3COOK gel with TiO_2/K_2O molar ratio of 6. The TG curve can be divided into three weight loss steps. The first weight loss (about 10%) at $T < 230$ °C is due to the volatilization of the free water and solvent. The second weight loss (about 30.6%) at 230–370 °C is quick. This step is due to the partial decomposition of organic substances and the reaction between $Ti(n\text{-}OC_4H_9)_4$ and CH_3COOK, corresponding to a broad exothermic peak centered at 300 °C on the DSC trace. The third 2.4 wt.% lost at 370–525 °C is relatively slow and steady, ending with a long step on the TG trace, which illustrates that organic solvents have been completely volatilized, but the reaction still continues. The TG trace became horizontal when $T > 525$ °C, there is no weight loss. But there is a weaker endothermic peak around at 625 °C on the DSC curve, at which point amorphous potassium hexatitanate converts to crystals. The peaks on the DSC trace at 300 and 625 °C are small, indicating that the intensities of the reaction and the phase change are weak.

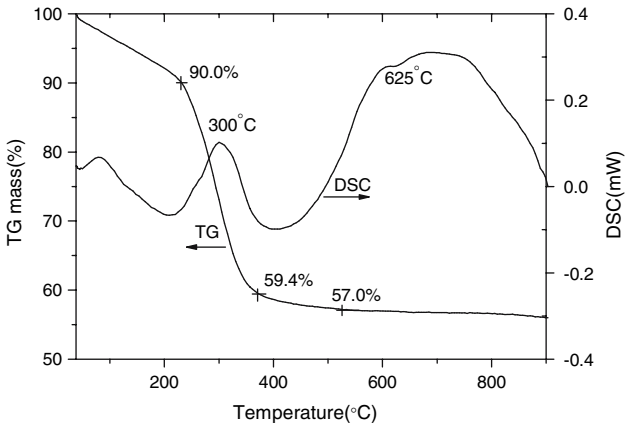

Fig. 1 TG-DSC curves of the $TiO_2/K_2O = 6$ (molar ratio) sol–gel

X-ray diffraction results

Figure 2 shows the results of X-ray diffraction patterns for CH_3COOK-$Ti(n\text{-}OC_4H_9)_4$ sol–gel samples sintered at different temperatures. There is only one peak with $2\theta = 5.9°$ at 100 °C, which is the characteristic peak of potassium polyacetate, Therefore, there is no reaction occurring at 100 °C. However, the diffraction peak of potassium polyacetate disappears completely when the sample was heated at 300 °C. This illustrates that the temperature of the reaction is lower than 300 °C. From thermodynamic calculations [21], the lowest reaction temperature between $TiO_2(nH_2O$ and K_2CO_3 is 300 °C during the solid state reaction process. The improvement of reaction activity and lower reaction temperature might attribute to the presence of a nano-scale mixing state between $TiO_2(nH_2O$ and K_2CO_3 [22]. The sol–gel method follows a soft chemistry mechanism and has lower the initial reaction temperature compared with solid state reaction.

In addition, all the samples annealed from 300 to 500 °C were amorphous. The broadening of the strongest XRD characteristic peak of $K_2Ti_6O_{13}$ at 600 °C indicates the formation of $K_2Ti_6O_{13}$ nanoclusters, but there is still a small amount of anatase. These agree with the results of TG-DSC. However, it can be seen that the characteristic peak of anatase disappears when the sintered temperature reaches 700 °C, revealing that anatase has been completely converted to potassium hexatitanate at 625 °C. This temperature also is lower than that of solid state reaction [23]. The width of the strongest characteristic peaks of $K_2Ti_6O_{13}$ becomes narrower with the increase of reaction temperature, indicating a crystal growth of potassium hexatitanate.

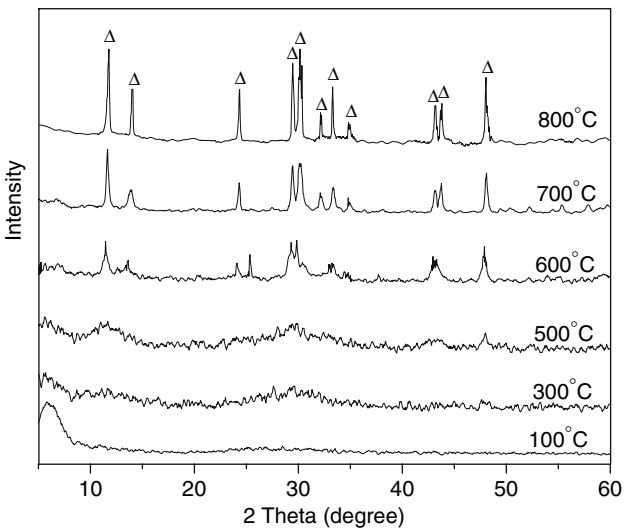

Fig. 2 XRD patterns of CH_3COOK-$Ti(n\text{-}OC_4H_9)_4$ sol–gel powder withTiO_2/K_2O molar ratio of 6 heated at different temperatures for 2 h

The increasing peak intensity for the same peak of potassium hexatitanate from 600 to 800 °C also indicates an increasing crystallinity of potassium hexatitanate with increasing reaction temperature.

Considering the heat-resistant temperature of ITO glass, we selected 600 °C as the optimum temperature of the preparation of potassium hexatitanate films. Figure 3 shows the XRD patterns of potassium titanate film calcined at 600 °C. It can be seen that all the characteristic peaks of $K_2Ti_6O_{13}$ appear. The characteristic peaks of anatase disappear completely, which disagrees with the XRD results of powder due to fewer amounts of materials on film.

According to the literature [23], for mixtures with TiO_2/K_2Omole ratio of 4, $K_2Ti_6O_{13}$ can be obtained with the loss of K_2O and residue of anatase at 640 °C during sintering process. However, $K_2Ti_6O_{13}$ film can be gained from CH_3COOK-Ti(n-$OC_4H_9)_4$ sol–gel with TiO_2/K_2O molar ratio of 6 heated at 600 °C, without the loss of K_2O and residue of anatase. This result shows the difference of reaction mechanism between sol–gel method and solid state reaction.

The crystal size derived from the (200) peak of $K_2Ti_6O_{13}$ with the Scherer equation is ca. 15 nm. The nano-crystallites can not only enhance the activity but also reduce the roughness of the films.

Raman spectra

Raman spectra of potassium titanate film on ITO glass are shown in Fig. 4. It can be seen that $K_2Ti_6O_{13}$ is the major components in Fig. 4. The Raman peaks of potassium hexatitanate agree with the previous report [24]. But the peak of 399 cm^{-1} has some broadening comparing with that of $K_2Ti_6O_{13}$ powder.

XRD and Raman results demonstrated the generation of $K_2Ti_6O_{13}$ after heated at 600 °C 2 h on films. However, when the powder mixtures were heated at 600 °C, the XRD diffraction peaks of $K_2Ti_6O_{13}$ and anatse appeared

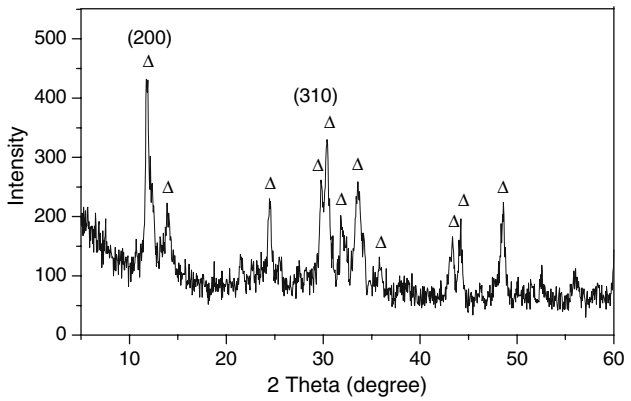

Fig. 3 XRD patterns of potassium titanate film calcined at 600 °C for 2 h

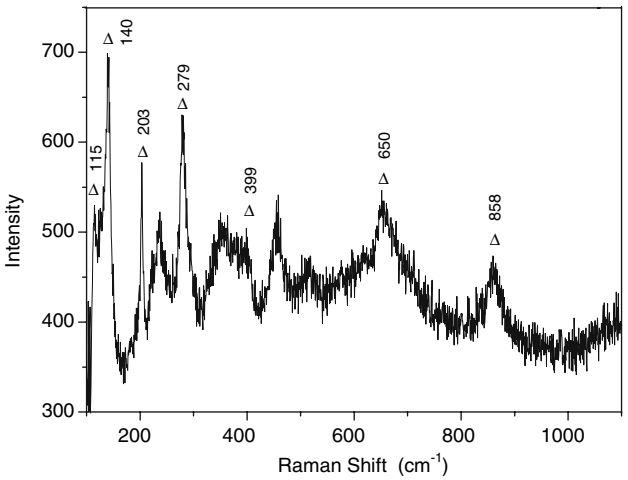

Fig. 4 Raman spectra of potassium titanate film heated at 600 °C for 2 h

simultaneously. The discrepancy can be attributed to the intervening of substrates and different formation mechanism of the films. The amount of material on film is much less than that of in powder, i.e., the whole process of nucleation and crystal growth of film is limited.

From the results of TG-DSC, XRD, and Raman, we conclude that the whole reaction process for preparing $K_2Ti_6O_{13}$ from CH_3COOK and Ti(n-$OC_4H_9)_4$ is as following:

$$2CH_3COOK + 6Ti(OC_4H_9) \overset{300\,^oC}{\rightarrow} K_2Ti_6O_{13}(\text{nuclei}) \overset{625\,^oC}{\rightarrow} K_2Ti_6O_{13}(\text{crystals})$$

Surface structure of potassium hexatitanate thin film

Cross-sectional SEM image of potassium hexatitanate film on Si(111) wafer sintered at 600 °C is shown in Fig. 5. It

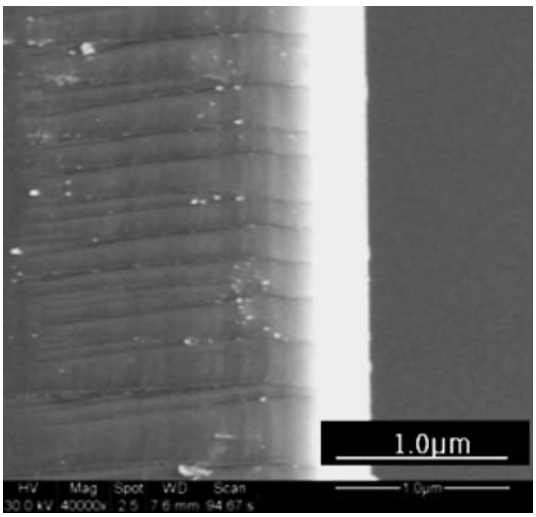

Fig. 5 Cross-sectional SEM images (six cycles) of potassium hexatitanate film on Si wafer sintered at 600 °C for 2 h

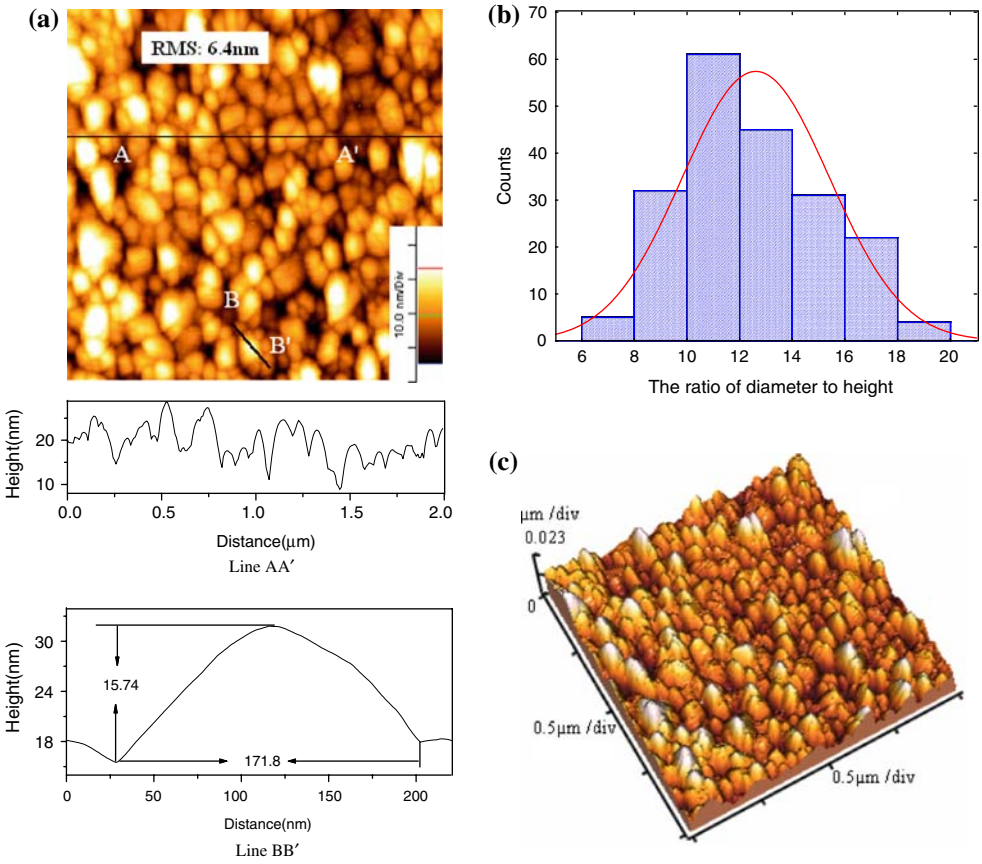

Fig. 6 2,000 nm × 2,000 nm 2D(**a**) and 3D(**c**) AFM images of $K_2Ti_6O_{13}$ films sintered at 600 °C. (**a**)-BB' shows a typical particle on the film. Histograms of the distribution of the ratio of the diameter to height for 200 particles (**b**) come from the analysis of topographic images

reveals that the film is dense, uniform and smooth, and its thickness is approximately 300 nm. The composition of the film analyzed by EDS attached to SEM shows strong characteristic peaks of K, Ti, O and Si.

Although many methods can be used to characterize the properties of potassium hexatitanate, AFM provides the surface microstructure and topography of potassium hexatitanate particles in films. Two-dimensional, three-dimensional and cross section AFM images of films are displayed in Fig. 6. The films consist of flat particles with sizes ranging typically from 80 to 180 nm. The surface is dense, uniform and smooth. There are some nanometer interspaces in the films. Compared with the XRD data, particles on the film are aggregation of nanocrystals because each layer was preheated one time at 350 °C for 10 min during the film deposition process, i.e., these bigger grains are second grain composed of many small potassium hexatitanate crystallites.

The cross sectional AFM segment, shown as an example, is the typical particle (Fig. 6a -BB'). The sizes of 200 particles from different AFM images on $K_2Ti_6O_{13}$ film shown in Fig. 6a, were measured to construct a histogram of particles distribution in Fig. 6b with the ratio of diameter to height of particles about 11. A narrow diameter/height distribution is observed in the samples and all samples have a similar average size, which illustrating that the growth mechanism of potassium hexatitanate nanocrystals on substrate is confined growth model in *Z*-axis direction. RMS roughness of the films measured on an area of 2,000 nm × 2,000 nm averaged out to 6.4 nm. The characteristic parameters of $K_2Ti_6O_{13}$ film are tabulated in Table 1.

The observation of TEM in Fig. 7a shows that the particles exhibit some small crystals with different size. The length of crystals is about 50–100 nm while the width is about 30–50 nm. These bigger grains are second grain composed of many small potassium hexatitanate crystallites.

Table 1 The characteristic parameters of $K_2Ti_6O_{13}$ film

Material (film)	Distribution of particles (200) (diameter/height)	Particles sizes (nm)	RMS (nm)	Thichness of film (nm)	Original grain size (from Scherer equation) (nm)
$K_2Ti_6O_{13}$	11	80–180	6.4	300	15

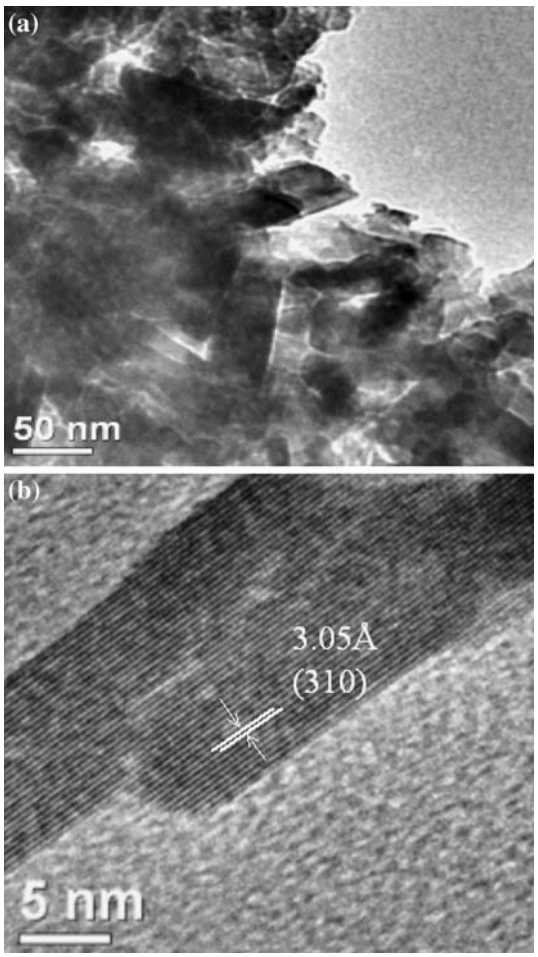

Fig. 7 TEM images of potassium titanate film heated at 600 °C. (**a**) topographic images (**b**) HREM image of a thin crystal platelet in films

This result agrees with the XRD measurement. Shown in Fig. 7b is a high resolution electron microscopy (HREM) image of a thin crystal platelet on the film. The structure appearing on the surface of the thin crystal platelet has a lattice spacing of about 3.05 Å, which corresponds to the (310) plane spacing of $K_2Ti_6O_{13}$. From this HREM image we can derive the conclusion that the thin crystal platelet is indeed $K_2Ti_6O_{13}$ [25].

Potoelectrochemical performance

Both wetting films and sintered films are compact and transparent on ITO glass.

Open circuit potential, photocurrent variations and photocurrent potential curves of potassium hexatitanate/ITO and titania/ITO films are shown in Fig. 8a–c, respectively. Figure 8a shows that the open circuit potentials of $K_2Ti_6O_{13}$ and titania film electrode (TiO_2: 1.35 V, $K_2Ti_6O_{13}$: 1.83 V) decreased rapidly down to lower values as a result of the sudden creation of electron-hole pairs in

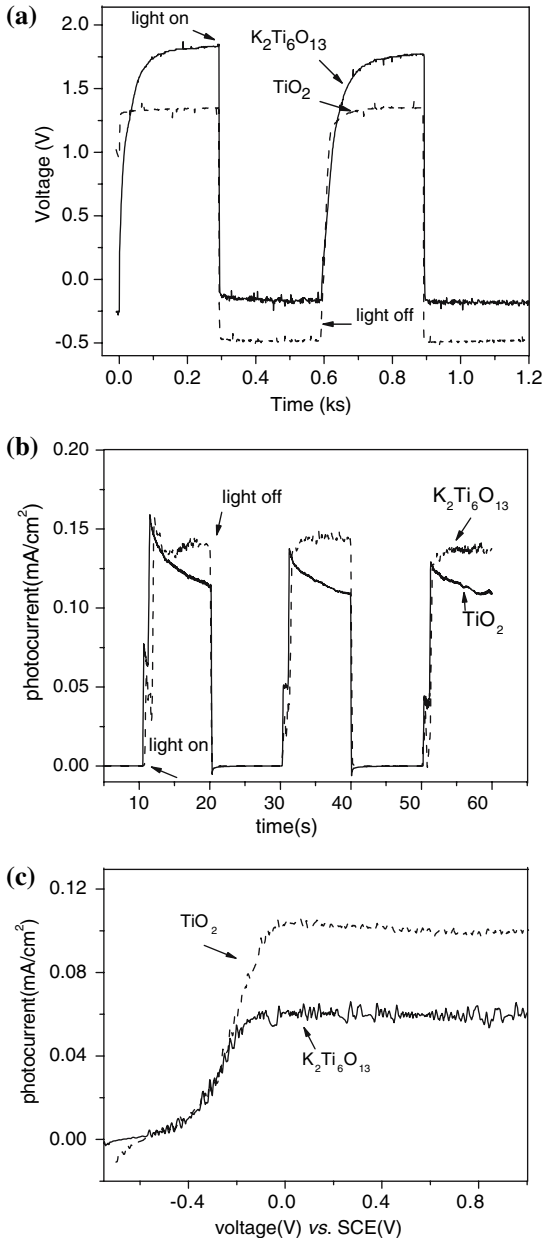

Fig. 8 Potoelectrochemical performance of $K_2Ti_6O_{13}$/ITO and titania/ITO films under UV light centered at 254 nm in 0.1 mol/l Na_2SO_4 solution. (**a**) Variation of open circuit potential with time. (**b**) Photocurrent curves. (**c**) Photocurrent-potential curves measured at 1 mVs^{-1} potential sweep rates

the films when the films were illuminated by UV light. The open circuit potential tended to stabilize and then attained a plateau (TiO_2: –0.48 V, $K_2Ti_6O_{13}$: –0.16 V). This negative charge is due to photogenerated electrons becoming trapped in the conduction band in the absence of an efficient electron acceptor, therefore raising the fermi potential of the electrode. In Fig. 8b, the photocurrent of film electrodes reached saturated state quickly when light turned on, but the photocurrent of TiO_2 electrode dropped steadily as

Table 2 Comparison of the photoelectrochemical properties of $K_2Ti_6O_{13}$ and TiO_2 film

Materials (film)	Photocurrent (mA/cm^2)	Open circuit potential (V vs.SCE)	Saturated photocurrent (mA/cm^2)	Potential of saturated photocurrent (V vs.SCE)
$K_2Ti_6O_{13}$	0.15	–0.16	–0.03	–0.15
TiO_2	0.15–0.11	–0.48	–0.10	–0.04

time proceeded when it reached saturated state due to the radical and electron scavenging properties of the O_2 at higher concentrations [26]. Gerischer [27] reported that O_2 acted as the electron acceptor and could produce O_2^- when it reacts with e^- during photoelectrochemical reactions. TiO_2 is shown that a sufficiently fast O_2 reduction rate [27], and resulting in the photocurrent of TiO_2 electrode dropping slowly. While $K_2Ti_6O_{13}$ film electrode possess a stable photocurrent.

It can be seen from Fig. 8c that an anodic photocurrent arises under UV illumination when the potential range is more positive than –0.5 V. As the positive potential increases, the resulting gradient within the films separates holes and electrons, decreasing their rate of recombination [28]. The photocurrent reaches a steady state after potential of –0.17 and –0.03 V (vs. SCE) for $K_2Ti_6O_{13}$ and TiO_2 film electrode, respectively, and in this case a maximum separation of the pair electron hole is obtained by the electric field. $K_2Ti_6O_{13}$ film electrode reaches saturated photocurrent prior to TiO_2 film electrode does, and its photocurrent was less than that of TiO_2 film. The most probable reasons for the difference are the variation in crystalline structure, specific surface, oxygen vacancies and electrical conductivity. A summary of the main data from the photoelectrochemical properties of $K_2Ti_6O_{13}$ and TiO_2 film electrodes is tabulated in Table 2.

Conclusions

The smooth potassium hexatitanate dense films with mesoscopic structures were synthesized via sol–gel method by controlling the molar ratio of CH_3COOK and $Ti(n\text{-}OC_4H_9)_4$ in sol. The reaction system of CH_3COOK- $Ti(n\text{-}OC_4H_9)_4$ sol–gel has been studied by TG-DSC, XRD, and Raman spectra. The starting temperature of this reaction system is lower than 300 °C and potassium hexatitanate nanocrystals were formed at 600 °C, with the original grain size about 15 nm. The smoothness at the nanometer scale of the films was obtained by means of AFM control. AFM topographic images analysis of the film presents the distribution of the ratio of the diameter to height of particles about 11. The film possesses smooth surface with RMS roughness value of 6.4 nm. HREM image of the films revealed a lattice spacing corresponding to the (310) plane spacing of $K_2Ti_6O_{13}$. The photoelectrochemical performance of $K_2Ti_6O_{13}$ film electrodes is similar to that of TiO_2 film. It is expected that the film could have better performance in alkaline solution and a potential application in alkaline cells.

Acknowledgement This work was supported by the National Natural Science Foundation of China (Grant Nos. 20246002 and 20236010), National High Technology Research and Development Program of China (No. 2003CB615700), the Key Science Foundation of Jiangsu Province, China (BK 2004215) and the Key Laboratory of Material-oriented Chemical Engineering of Ministry of Education, China.

References

1. Urban JJ, Yun WS, Gu Q, Park H (2002) J Am Chem Soc 124:1186
2. Zhu HY, Lan Y, Gao XP, Ringer SP, Zheng ZF, Song DY, Zhao JC (2005) J Am Chem Soc 127:6730
3. Ma R, Fukuda K, Sasaki T, Osada M, Bando Y (2005) J Phys Chem B 109:6210
4. Du GH, Chen Q, Han PD, Yu Y, Peng LM (2003) Phys Rev 67:035323
5. Corcoran DJ, Tunstall DP, Irvine JT (2000) Solid State Ionics 136/137:297
6. Bao N, Lu X, Ji X, Feng X, Xie J (2002) Fluid Phase Equilib 193(1–2):229
7. Choy JH, Lee HC, Jung H, Huang SJ (2001) J Mater Chem 11:2232
8. He M, Feng X, Lu X, Ji X, Liu CH, Bao N, Xie J (2004) J Mater Sci 39:1
9. Ogawa M, Kuroda K (1995) Chem Rev 95:399
10. Yahya RB, Hayashi H, Nagase T, Ebina T, Onodera Y, Saitoh N (2001) Chem Mater 13:842
11. Yang Z, Bao N, Liu CH, Feng X, Xie J, Ji X, Lu X (2002) Chem J Chinese U 23:1371
12. Airdoldi C, Nunes LM, Farias RF (2000) Mater Res Bull 35:2081
13. Li JH, Ning XG, Ye HQ, Pan J, Fukunaga H (1997) J Mater Sci 32:543
14. Feng X, LV J, Lu X, Bao N, Ceng D (1999) Acta Mater Comp Sinica 16:1
15. Ogura S, Kohno M, Sato K, Inoue Y (1997) Appl Surf Sci 121/122:521
16. Lee HK, Shim JP, Shim MJ, Kim SW, Lee JS (1996) Mater Chem Phys 45:243
17. Barnes MC, Kumar S, Green L, Hwang NM, Andrea GR (2005) Surf Coat Technol 190(2–3):321
18. Sandell A, Anderson MP, Alfredsson Y (2002) J Appl Phys 92(6):3381
19. Hench LL, West JK (1990) Chem Rev 90(1):33
20. Sammelselg V, Rosental A, Tarre A (1998) Appl Surf Sci 134(1–4):78
21. Bao N, Feng X, Lu X, Shen L, Yanagisawa K (2004) AIChE J 50:1568
22. Yu L, He M, Liu C, Lu X, Feng X (2005) Mater Chem Phys 93:342

23. Liu C, Lu X, Yu G, Feng X, Zhang Q, Xu Z (2005) Mater Chem Phys 94:401
24. Bamberger CE, Begun GM, Macdougall CS (1990) Appl Spectrosc 44:30
25. Du GH, Chen Q, Han PD, Yu Y, Peng LM (2003) Phys Rev 67:035323
26. Byrne JA, Davidson A, Dunlop PSM, Eggins BR (2002) J Photochem Photobiol A: Chem 148:365
27. Gerischer H, Heller A (1991) J Phys Chem 95:5261
28. Leng WH, Zhang Z, Zhang JQ, Cao CN (2005) J Phys Chem B 109(31):5008